Studies of light mesons at COMPASS

Sebastian Uhl[1,a,b], on behalf of the COMPASS Collaboration

[1] *Technische Universität München, James-Franck-Straße, 85748 Garching, Germany*

Abstract. COMPASS is a fixed-target experiment at the CERN SPS aimed at the study of the structure and dynamics of hadrons. The two-stage spectrometer has a good acceptance over a wide kinematic range for charged as well as neutral particles and thus allows the access to a wide range of reactions. Data with negative hadron beams of $190 \, \mathrm{GeV}/c$, consisting mainly of pions, have been taken to study in particular light mesons. Their spectrum is investigated in diffractive dissociation reactions at squared four-momentum transfer to the target between 0.1 and $1.0 \, (\mathrm{GeV}/c)^2$ with final states containing pions and η mesons. The flagship channel is the $\pi^-\pi^+\pi^-$ final state, for which COMPASS has recorded the at present world's largest data sample. A new axial-vector meson, the $a_1(1420)$, has been found with unusual properties, pointing to an exotic nature. Novel analysis techniques are developed to extract the amplitude of the $\pi^+\pi^-$ sub-system as a function of 3π mass from the data. The findings are confirmed by the analysis of the $\pi^-\pi^0\pi^0$ final state.

1 Introduction

The **Co**mmon **M**uon and **P**roton **A**pparatus for **S**tructure and **S**pectroscopy (COMPASS) experiment is a fixed-target experiment located at CERN's Super Proton Synchrotron (SPS). One of its goals is to study the spectrum of light mesons. A $190 \, \mathrm{GeV}/c$ negative hadron beam, consisting mostly of pions with a small admixture of kaons and anti-protons, impinges on a liquid hydrogen target, and diffractively produces the mesons under study. The decay products of these mesons are detected in a two-stage magnetic spectrometer (figure 1). Each of the two spectrometer stages is equipped with an electromagnetic calorimeter. This setup provides full coverage for charged and neutral particles, resulting in a homogenous acceptance over a wide kinematic range [1].

The reaction under study here is the diffractive production of mesons decaying into three pions, either into the $\pi^-\pi^-\pi^+$ or the $\pi^-\pi^0\pi^0$ final state. To this end, exclusive events with a squared four-momentum transfer to the target t' between $0.1 \, \mathrm{GeV}/c^2$ and $1.0 \, \mathrm{GeV}/c^2$ have been selected in a three-pion mass range between $0.5 \, \mathrm{GeV}/c^2$ and $2.5 \, \mathrm{GeV}/c^2$. This results in a huge dataset of 50 million $\pi^-\pi^-\pi^+$ and 3.5 million $\pi^-\pi^0\pi^0$ events. The invariant mass distributions of the two final states (figure 2) indicate a rich spectrum of contributing states.
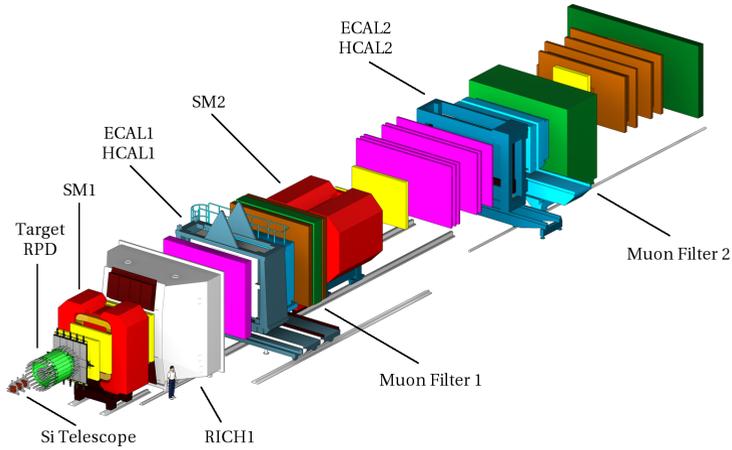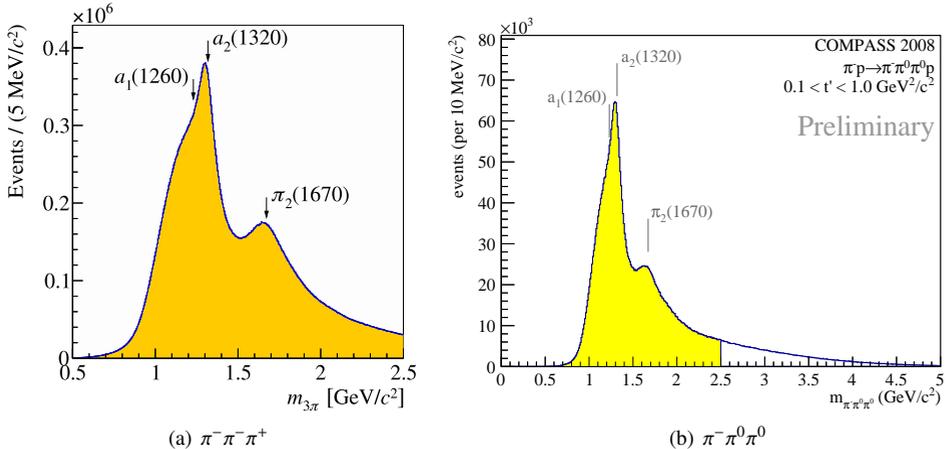
Figure 1. Sketch of the experimental setup. The beam enters the experiment from the lower left corner of the figure. (Figure from [1].)

Figure 2. Invariant mass spectra of the two studied final states. (Figure (a) from [2].)

2 Partial-wave analysis

To decompose the three-pion mass spectra into the individual spin-parity components, a partial-wave analysis employing the isobar model is used. Figure 3 sketches the process under study. The incoming beam π^- diffractively scatters off a target proton producing an intermediate state X^-, which subsequently decays into a two-pion isobar $R_{\pi\pi}$ and a bachelor pion which have a relative orbital angular momentum L. The two-pion isobar then decays into two pions. By exploiting the kinematic distribution in the five phase-space variables of the decay products, information on the spin J, the parity P, and the spin-projection M^ε of X^- can be extracted [2].
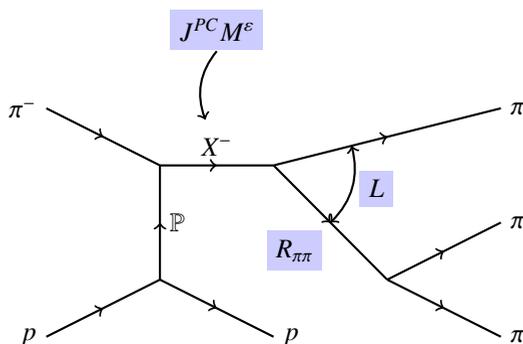
Figure 3. Sketch of the process under study.

(a) $\pi^-\pi^0$ mass spectrum
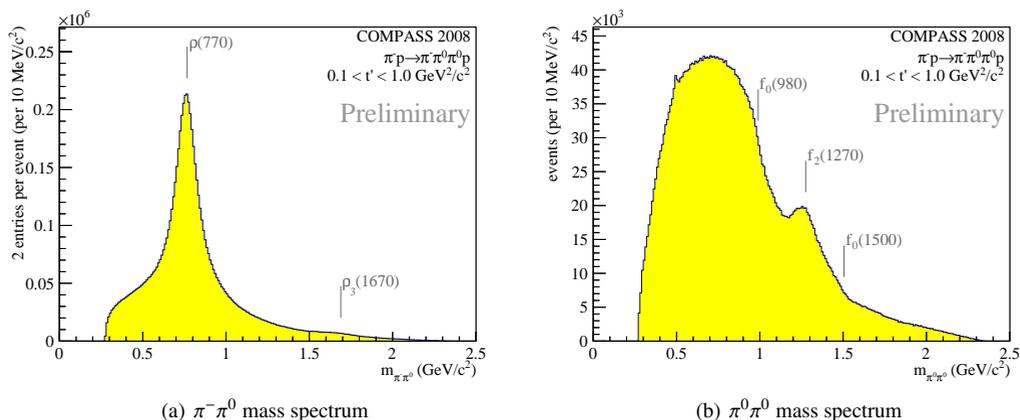
(b) $\pi^0\pi^0$ mass spectrum

Figure 4. Invariant mass spectra of the two possible two-pion subsystems of the $\pi^-\pi^0\pi^0$ final state.

The mass spectra of the two-pion isobars of the $\pi^-\pi^0\pi^0$ final state are shown in figure 4. The isobars decaying to $\pi^-\pi^0$ have isospin $I = 1$. The $\rho(770)$ is clearly visible in figure 4(a). A smaller shoulder at higher masses suggests to also use the $\rho_3(1690)$. The $\pi^0\pi^0$ isobars have isospin $I = 0$. Here the $f_0(980)$, the $f_2(1270)$, and the $f_0(1500)$ are identified by bumps and kinks on top of a broad $(\pi\pi)_S$ component in figure 4(b). For the $\pi^-\pi^-\pi^+$ final state the two different isospin contributions cannot be separated. All isobars are $\pi^-\pi^+$ isobars. The same isobars as for the $\pi^-\pi^0\pi^0$ final state are used.

Each partial wave corresponds to one state X^- with its quantum numbers $J^{PC}M^\varepsilon$ decaying via one particular decay chain $R_{\pi\pi}\,\pi\,L$. For the analyses presented in the following, states with spin J up to 6 are included. Also the angular momentum L between the isobar $R_{\pi\pi}$ and the bachelor pion can go up to 6. Out of the possible combinations, 87 waves with non-negligible intensity are kept for the final model: 80 waves with a positive reflectivity $\varepsilon = +1$ and 7 with $\varepsilon = -1$. In addition one incoherent wave with an isotropic angular distribution is included [2]. The same set of partial waves is used in the two analyses of the different final states.

(a) $2^{++}1^+\rho(770)\,\pi D$

(b) $4^{++}1^+\rho(770)\,\pi G$
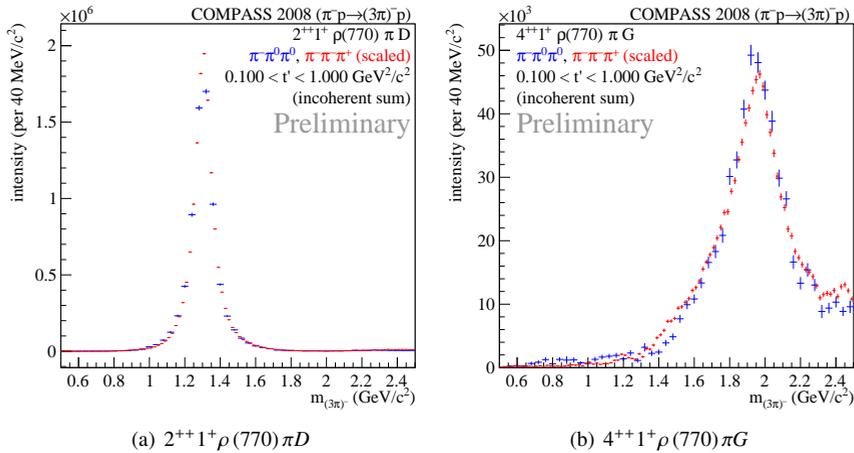
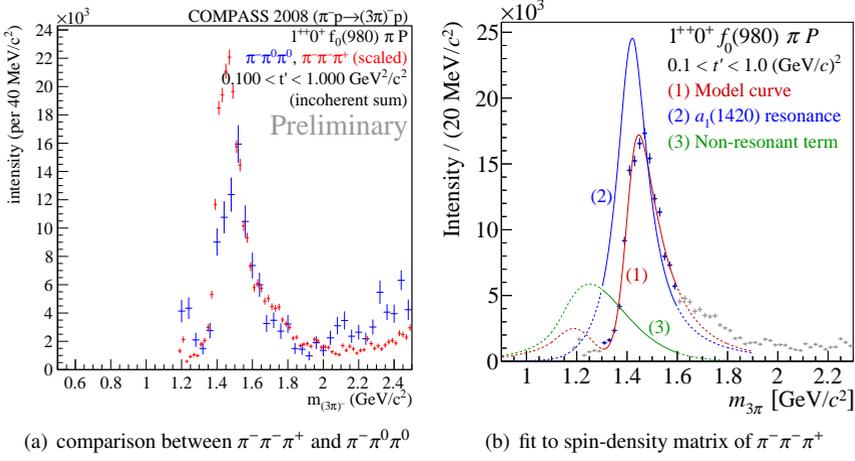**Figure 5.** Incoherent sum of partial-wave intensities over all t' bins.

3 Fit in mass bins

As a first step, the partial-wave intensities are extracted in bins of the three-pion mass and the squared four-momentum transfer to the target t' using a rank-1 fit. Figure 5 shows the incoherent sum of the intensities over the individual t' bins for the $2^{++}1^+\rho(770)\,\pi D$ wave, clearly showing the $a_2(1320)$, and the $4^{++}1^+\rho(770)\,\pi G$ wave, clearly showing the $a_4(2040)$. The results from the $\pi^-\pi^-\pi^+$ channel (red markers) and the $\pi^-\pi^0\pi^0$ channel (blue markers) are in agreement. The two data sets are normalized using the intensity integrals in each individual plot so that the peak shapes can directly be compared. No dependence of the peak shapes on the squared four-momentum transfer t' is observed for these two partial waves. Good agreement of the partial-wave intensities between the two final states is also found for other waves with large intensities, like the $1^{++}0^+\rho(770)\,\pi S$ and $2^{-+}0^+ f_2(1270)\,\pi S$ waves [3].
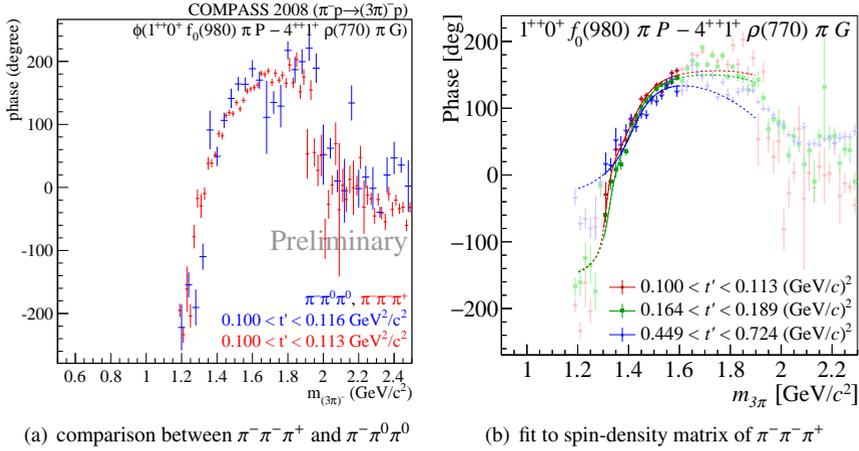
Also for waves with small intensities good agreement between the two final states is observed. One particularly interesting signal is observed in the $1^{++}0^+ f_0(980)\,\pi P$ wave (figure 6) around $1.4\,\mathrm{GeV}/c^2$. This narrow structure, never observed before, could correspond to a possible new a_1 state. It is seen in the decay via the $f_0(980)$ isobar for both channels and for all t' bins. Different parameterizations for the isobars have been tested to exclude a possible artifact from the employed model.

In addition to the intensities, also the phase difference between partial waves needs to be considered for a resonant interpretation of this signal. Figure 7 shows the phase difference between the $1^{++}0^+ f_0(980)\,\pi P$ and the $4^{++}1^+\rho(770)\,\pi G$ wave. A clear phase motion around $1.4\,\mathrm{GeV}/c^2$ is visible at the position of the peak in the intensity spectrum.

In order to exclude possible artifacts caused by the particular choice for the parametrization of the isoscalar $J^{PC} = 0^{++}$ isobars, a partial-wave analysis was performed, in which the waves with $(\pi\pi)_S$, $f_0(980)$, and $f_0(1500)$ isobars are replaced by amplitudes piecewise constant in the two-pion mass [2]. This new approach allows a rather model-independent extraction of the 0^{++} isobar amplitudes. The analysis shows a clear correlation between the new $a_1(1420)$ signal and the $f_0(980)$ as a decay product.

(a) comparison between $\pi^-\pi^-\pi^+$ and $\pi^-\pi^0\pi^0$

(b) fit to spin-density matrix of $\pi^-\pi^-\pi^+$

Figure 6. Incoherent sum of partial-wave intensities over all t' bins of the $1^{++}0^+ f_0(980)\,\pi P$ wave. (Figure (b) from [4].)

(a) comparison between $\pi^-\pi^-\pi^+$ and $\pi^-\pi^0\pi^0$

(b) fit to spin-density matrix of $\pi^-\pi^-\pi^+$

Figure 7. Phase difference between the $1^{++}0^+ f_0(980)\,\pi P$ and the $4^{++}1^+ \rho(770)\,\pi G$ wave (a) for the lowest t' bins of the $\pi^-\pi^-\pi^+$ and $\pi^-\pi^0\pi^0$ final states , and (b) with a fit to the spin-density matrix of the $\pi^-\pi^-\pi^+$ final state. (Figure (b) from [4].)

4 Fit to spin-density matrix

To further study this new signal, and to extract Breit-Wigner parameters, the mass dependence of a sub-set of the spin-density matrix was extracted for the $\pi^-\pi^-\pi^+$ channel [4]. Apart from the intensities, also the interferences between the waves were taken into account. The three waves shown in figures 5 and 6 were used. The fit model included one Breit-Wigner resonance in each wave: the $a_2(1320)$ in the $2^{++}1^+\rho(770)\,\pi D$ wave, the $a_4(2040)$ in the $4^{++}1^+\rho(770)\,\pi G$ wave, and a new $a_1(1420)$ in the $1^{++}0^+ f_0(980)\,\pi P$ wave. The Breit-Wigner parameters were extracted from a simultaneous fit to the

spin-density submatrices of the three partial waves in all eleven t' bins. Apart from the Breit-Wigner components used to describe the resonances, also a coherent t'-dependent non-resonant contribution was allowed in each wave. The parameters of the Breit-Wigner functions and the coherent background were the same in all t' bins, only the complex couplings were allowed to differ.

The partial-wave intensity of the $1^{++}0^+ f_0 (980) \pi P$ wave (blue markers in figure 6(b)) is described by a resonant contribution for the new $a_1 (1420)$ (blue line) interfering with a non-resonant contribution (green line). The total intensity of the model is shown by the red line. The fit range is indicated by a full line, the dashed line shows the extrapolation beyond the range. Figure 7(b) shows the interference between the $1^{++}0^+ f_0 (980) \pi P$ wave and the $4^{++}1^+ \rho (770) \pi G$ wave. The three different colors show three of the in total eleven t' bins. Again the markers show the result from the partial-wave decomposition, while the lines show the behaviour of the resonance model. The parameters of the Breit-Wigner function describing the new $a_1 (1420)$ are $M = 1414 \, \mathrm{MeV}/c^2$ with a systematic error of $^{+15}_{-13} \, \mathrm{MeV}/c^2$ for the mass, and $\Gamma = 153 \, \mathrm{MeV}/c^2$ with a systematic error of $^{+8}_{-23} \, \mathrm{MeV}/c^2$ for the width. The statistical errors are negligible.

5 Conclusions

The COMPASS experiment has recorded a huge dataset to study resonances produced in diffractive dissociation into three pions. The large number of events allowed to increase the number of waves used in the partial-wave analysis, while still being able to also perform a t'-dependent analysis. Breit-Wigner parameters have been extracted from a fit to the result of the spin-parity decomposition in mass bins. Apart from the well-known resonances, COMPASS found a new signal in the $1^{++}0^+ f_0 (980) \pi P$ wave around $1.4 \, \mathrm{GeV}/c^2$. It is a rather narrow object featuring a well-defined mass and width, and appears only in the $f_0 (980)$ decay mode. Its nature is still unclear, it could be the isospin partner of the $f_1 (1420)$, but also other explanations have been put forward. The $a_1 (1420)$ could be a genuine resonance as a two-quark-tetraquark mixed state [5]. Also two explanations connecting the new $a_1 (1420)$ to the known $a_1 (1260)$ are proposed. The first explains the observed intensity spectra and phases in the $1^{++}0^+ f_0 (980) \pi P$ wave by a two-channel unitarized Deck amplitude interfering with the direct production of the $a_1 (1260)$ [6]. The second explains those by a singularity in a triangle diagram describing rescattering in the $K^- \bar{K}^*$ decay of the $a_1 (1260)$ [7].

References

[1] COMPASS collaboration, P. Abbon *et al.*, NIM A**779**, 69 (2015), arXiv:1410.1797.
[2] COMPASS collaboration, C. Adolph *et al.*, submitted to Phys. Rev. D, arXiv:1509.00992.
[3] S. Uhl on behalf of the COMPASS Collaboration, PoS(Hadron 2013)087, arXiv:1401.4943.
[4] COMPASS collaboration, C. Adolph *et al.*, Phys. Rev. Lett. **115**, 082001 (2015), arXiv:1501.05732.
[5] Z.G. Wang, arXiv:1401.1134.
[6] J.L. Basdevant, E. Berger, Phys. Rev. Lett. **19**, 192001 (2015).
[7] M. Mikhasenko, B. Ketzer, A. Sarantsev, Phys. Rev. D**91**, 094015 (2015).